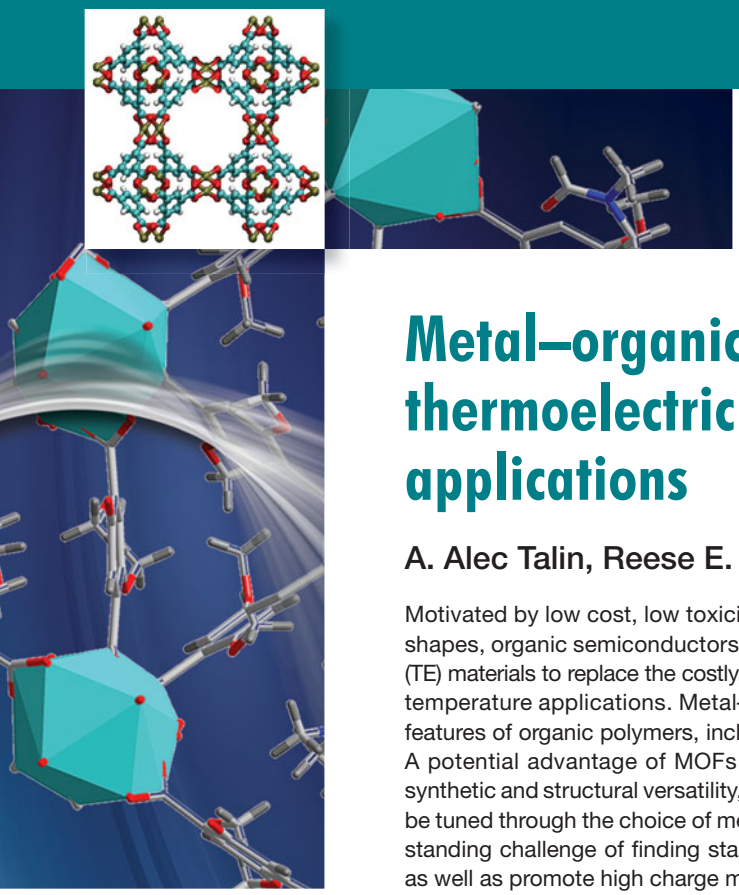

Metal–organic frameworks for thermoelectric energy-conversion applications

A. Alec Talin, Reese E. Jones, and Patrick E. Hopkins

Motivated by low cost, low toxicity, mechanical flexibility, and conformability over complex shapes, organic semiconductors are currently being actively investigated as thermoelectric (TE) materials to replace the costly, brittle, and non-eco-friendly inorganic TEs for near-ambient-temperature applications. Metal–organic frameworks (MOFs) share many of the attractive features of organic polymers, including solution processability and low thermal conductivity. A potential advantage of MOFs and MOFs with guest molecules (Guest@MOFs) is their synthetic and structural versatility, which allows both the electronic and geometric structure to be tuned through the choice of metal, ligand, and guest molecules. This could solve the long-standing challenge of finding stable, high-TE-performance *n*-type organic semiconductors, as well as promote high charge mobility via the long-range crystalline order inherent in these materials. In this article, we review recent advances in the synthesis of MOF and Guest@MOF TEs and discuss how the Seebeck coefficient, electrical conductivity, and thermal conductivity could be tuned to further optimize TE performance.

Introduction

When two parts of an electric conductor are held at different temperatures, charge carriers diffuse from the hot to the cold regions, producing a voltage difference that is the basis for the thermoelectric (TE) Seebeck effect. The Seebeck coefficient, S, is the voltage difference resulting from a temperature gradient and a measure of thermopower. It can be positive (for hole conductors) or negative (for electron conductors), ranging from a few μV/K, typically for metals, to more than 1000 μV/K, observed in lightly doped semiconductors.[1] A TE generator (TEG) is a solid-state device that takes advantage of the Seebeck effect to directly convert a temperature gradient into electricity.

The efficiency of a TE conversion device is determined by the figure of merit of the materials comprising the device:

$$ZT = \frac{S^2 \sigma T}{\kappa}, \qquad (1)$$

where σ is the electrical conductivity, T is the average temperature, κ is the thermal conductivity, and $S^2\sigma$ (W/mK^2) is the power factor (PF) of the material. Materials that combine high values of S and σ/κ are therefore attractive for TE applications. There is no theoretical limit on the value of ZT; however, finding materials with ZT significantly greater than 1 is challenging due to the interdependencies that exist among the parameters.

A large S requires that σ (or electronic density of states) near the Fermi level E_F change rapidly,[2] as indicated by the Mott expression for S:

$$S = \frac{\pi^2}{3}\frac{k_B}{q}k_B T\left\{\frac{d\left(\ln\left[\sigma(E)\right]\right)}{dE}\right\}_{E=E_F}, \qquad (2)$$

where k_B is the Boltzmann constant, and q is the elementary charge. Materials such as lightly doped semiconductors for which the density of states at the Fermi level, $n(E)_{E=E_F}$, changes rapidly with energy are expected to have large S values; however, such materials also tend to be poor electrical conductors since the free-carrier concentration is low, and therefore, the ZT factor is low. A compromise between maximizing S and σ favors low-bandgap semiconductors (doping ~10^{19}–10^{21}/cm^3), such as Bi_2Te_3 and its alloys.

Designing materials with optimum ZT is further complicated by the relationship between κ and σ. κ is the sum of lattice

A. Alec Talin, Sandia National Laboratories, USA; aatalin@sandia.gov
Reese E. Jones, Sandia National Laboratories, USA; rjones@sandia.gov
Patrick E. Hopkins, Department of Mechanical and Aerospace Engineering, University of Virginia, USA; phopkins@virginia.edu
doi:10.1557/mrs.2016.242

thermal conductivity, κ_l, and the electronic thermal conductivity, κ_e. According to the Wiedemann-Franz Law, $\kappa_e/\sigma = LT$, where the Lorenz number $L = 2.4 \times 10^{-8}$ $J^2K^{-2}C^{-2}$ for a free-electron metal. For semiconductors with relatively low free-carrier concentrations ($<10^{-19}$/cm^3), κ is dominated by the lattice contribution. Weathers et al.[3] and Liu et al.[4] recently demonstrated that, as electronic carrier concentration and mobility increase, so does κ_e, including in the case of conducting polymers such as poly(3,4-ethylenedioxythiophene) (PEDOT). Hence another major thrust in TE material engineering is minimizing the lattice contribution, κ_l, to achieve the lowest total thermal conductivity κ and a maximal *PF*.

Thermoelectric materials

Inorganic semiconductors such as Bi_2Te_3 and some of its alloys with Sb and Sn (see **Table I**)[5,6] have adequate efficiency for a variety of niche applications,[7,8] but have not been widely adopted because they are difficult to deposit over complex or high-surface-area structures, can be toxic, and are too expensive for many applications. Nanostructuring and superlattices have yielded structures with $ZT > 2$, but these complex materials still remain impractical and too expensive for widespread applications such as integration with solar cells or for powering wearable electronics/sensors powered by body heat.[9]

As an alternative to inorganic materials, conducting polymers have recently attracted attention for TE applications, motivated by their low material cost, ease of processability, nontoxicity, mechanical flexibility, and low thermal conductivity.[10–12] Conducting polymers such as polyacetylene, polyaniline, polypyrrole, and PEDOT consist of long, conjugated molecular chains with varying degree of crystallinity.[13] In virtually all cases, obtaining significant σ in polymers requires doping. The dopants are typically organic or inorganic acids that remove electrons from the valence band of the polymers, but are themselves insulators that can occupy significant volume fraction, as well as cause structural disorder, decrease chain-to-chain electronic coupling, and depress carrier mobility.[14] Minimizing the dopant volume and exercising precise control of the oxidation state recently yielded PEDOT:PSS (PSS = polystyrene sulfonate) with a *PF* of 480 $\mu Wm^{-1}K^{-2}$.[15] However, the interpretation of this result was confounded by the fact that σ and κ were not measured for the same specimens or in the same direction with respect to the specimen geometry.[3]

TEGs require both *p*- and *n*-type elements arranged such that holes and electrons flowing from the hot to cold ends recombine to generate a current (**Figure 1**a). Unfortunately, achieving chemically stable *n*-type conducting polymers is challenging because the position of the lowest unoccupied molecular orbital (LUMO) level relative to the vacuum level (i.e., the electron affinity [EA]) is low for most linear chain-conjugated organic polymers.[16] Recently, electron-deficient conjugated systems with EA below –4.0 eV have emerged, but the best performing among these, benzodifurandion poly(*p*-phenylene vinylene) (BDPPV) doped with N-DMBI N-([4-(1,3-dimethyl-2,3-dihydro-1*H*-benzoimidazol-2-yl) phenyl]dimethylamine), yielded a *PF* of 0.28×10^{-4} $Wm^{-1}K^{-2}$, well below the values achieved for *p*-type polymers.

An alternative approach is to consider coordination polymers (CPs), which are composed of repeating units of metal–organic coordination complexes. Unlike all-organic conjugated polymers for which the valence and conduction bands are associated with the delocalized π and π^* orbitals of the carbon backbone, respectively, the electronic structure of CPs is dominated by the transition-metal *d* electrons and their interaction with the organic ligands.[17,18] In fact, the CP poly(K_x[Ni-ett]), composed of Ni(II) ions coordinated to 1,1,2,2-ethenetetrathiolate (ett) with potassium used to balance the charge, currently holds the record as the *n*-type polymer with the highest *ZT* at room temperature. Unfortunately, a solution-based processing route to poly(K_x[Ni-ett]), which is particularly suitable for mass production, has not yet been demonstrated.

Conducting metal–organic frameworks as thermoelectrics

Metal–organic frameworks (MOFs) share many of the advantages of all–organic polymer TEs for applications requiring large-area processable, nontoxic, and low-cost materials. Additionally, MOFs and MOFs with guest molecules (Guest@MOF) materials offer higher thermal stability (up to ~400°C in some cases) and have long-range crystalline order, which could be harnessed to improve charge mobility. MOFs offer

Table I. Thermoelectric properties of selected materials.

Material	Type	σ (S/m)	κ (W/mK)	*S* (μV/K)	*PF* (μW/mK²)	*ZT*	Reference
$Bi_{0.5}Sb_{1.5}Te_3$	*p*	1.2×10^5	1.4	185	4500	1.2	7
$Bi_2Te_{2.7}Se_{0.3}$	*n*	1.2×10^5	1.0	–180	2500	0.7	8
PEDOT:PSS	*p*	9×10^5	0.24	76	480	0.42	15
Poly(Cu_x[Cu-ett])	*p*	9×10^3	0.52	55	25	0.015	5
Poly(K_x[Ni-ett])	*n*	4×10^3	0.2	–125	26	0.1	6
TCNQ@Cu_3(BTC)$_2$	*p*	0.45	0.25	400	0.06	10^{-4}	19

Note: PEDOT, poly(3,4-ethylenedioxythiophene); PSS, polystyrene sulfonate; ett, 1,1,2,2-ethenetetrathiolate; TCNQ, tetracyanoquinodimethane; BTC, benzene 1,3,5-tricarboxylate; σ, electrical conductivity; κ, thermal conductivity; *S*, Seebeck coefficient; *PF*, power factor; *ZT*, figure of merit.

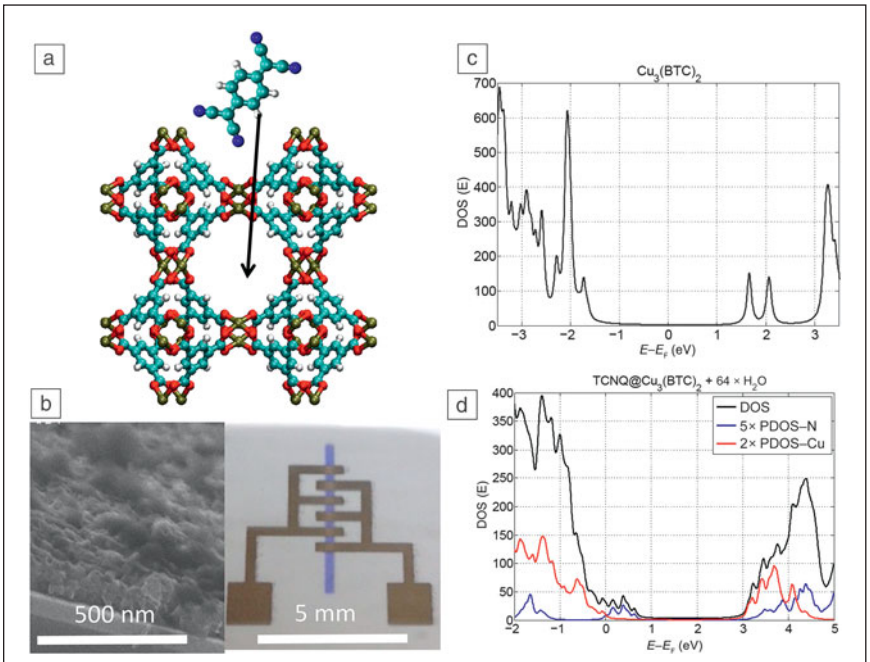

Figure 1. (a) Tetracyanoquinodimethane (TCNQ) above a $Cu_3(BTC)_2$ with arrow pointing to the pore. Color code: white, H; blue, N; cyan, C; red, O; ochre (light brown), Cu. Reprinted with permission from Reference 21. © 2013 Wiley. (b) (left) Scanning electron microscope image of $Cu_3(BTC)_2$ deposited using liquid-phase layer-by-layer growth and (right) an optical image of $Cu_3(BTC)_2$ (blue line) with Ag electrodes all deposited on paper by inkjet printing. (c) Electronic density of states (DOS) calculated *ab initio*—for $Cu_3(BTC)_2$ E_F is in the electronic gap. (d) For $TCNQ@Cu_3(BTC)_2$, E_F is near the metal–organic framework (MOF) valence band. The blue curve indicates the partial density of states (PDOS) obtained by projecting the wave functions on the TCNQ N atoms, while the red curve indicates the PDOS obtained by a similar projection on the MOF Cu atoms. Despite the relatively large Seebeck coefficient, the electrical conductivity and the power factor need to increase by ~10^3 for practical applications. Reprinted with permission from Reference 24. © 1999 Taylor & Francis. Note: BTC, benzene 1,3,5-tricarboxylate; *E*, energy; E_F, Fermi energy.

tremendous synthetic and structural versatility for optimizing the electronic structure for high *p*- and *n*-type *ZT* through appropriate choices of metal and ligand. The long-range crystalline order of MOFs promotes high-charge mobility to increase σ without adversely affecting *S*. A further aspect that differentiates MOFs from the broader class of nonporous CPs is their ability to adsorb a large variety of molecules and nanostructures within their pores to further tune or dramatically change the material's electronic and thermal-transport characteristics (see the article by Allendorf et al. in this issue). The field of MOF-based TEs is still in its infancy, however, and to date, only one MOF has been explored for TE applications: the $TCNQ@Cu_3(BTC)_2$ Guest@MOF system (TCNQ, tetracyanoquinodimethane; BTC, benzene 1,3,5-tricarboxylate).[19]

$TCNQ@Cu_3(BTC)_2$ thermoelectric

The $Cu_3(BTC)_2$ MOF forms face-centered-cubic crystals consisting of Cu(II) dimers coordinated by four BTC linkers (Figure 1a). The $Cu_3(BTC)_2$ MOF can be deposited by a variety of methods, including solution-based thin-film growth and inkjet printing.[20,21] The latter is particularly attractive for low-cost TE fabrication since relatively thick layers with desired pattern and current collectors can be rapidly deposited on low-cost substrates such as paper and fabrics, as demonstrated in Reference 21 and in our laboratory (Figure 1b, right-hand side).

When $Cu_3(BTC)_2$ is infiltrated with TCNQ, the TCNQ molecules bridge the Cu(II) dimers, forming $TCNQ@Cu_3(BTC)_2$ and an electronic conduction pathway and increasing σ from $<10^{-9}$ S/m to ~0.1 S/m.[20] When a thin film of $TCNQ@Cu_3(BTC)_2$ is placed onto a stage with a thermal gradient, a positive voltage is measured between the cold and hot sides (see **Figure 2**a–b) with $S \sim 400$ μV/K at room temperature (Figure 2c–d), indicating that holes are the dominant electronic charge carriers in the infiltrated framework.

The positive *S* is consistent with the calculated density of states that shows how E_F in $Cu_3(BTC)_2$ moves from the mid-gap to the valence band upon infiltration with TCNQ (Figure 1c–d). This can be rationalized by the fact that the LUMO levels of TCNQ lie close to the $Cu_3(BTC)_2$ valence band due to the large electron affinity of TCNQ. The blue line in Figure 1d indicates that the TCNQ LUMO levels are situated just above E_F, whereas the $Cu_3(BTC)_2$ valence band (red line) is located just below E_F. Despite the large *S*, the relatively low σ results in a comparatively low *PF* of ~0.06 μW/mK^2 (see Table I for comparison).

To determine the figure of merit *ZT*, κ for $TCNQ@Cu_3(BTC)_2$ was measured using time-domain thermoreflectance (TDTR). This is an optical pump-probe technique that utilizes ultrafast laser pulses (typically sub-picosecond) to monitor the surface temperature of a sample as a function of time. In TDTR, a modulated train of pump pulses heats the sample, creating both a time- and frequency-domain heating event in the sample of interest, and probe pulses, which are time delayed relative to the pump pulses, monitor the change in reflectivity of the sample surface, which is related to the temperature change.[22] The TDTR measurements on the $TCNQ@Cu_3(BTC)_2$ sample yielded a room-temperature value of 0.27 ± 0.04 $Wm^{-1}K^{-1}$.[19] This low κ value, which helps maximize the figure of merit in Equation 1 with all other factors being equal, is comparable to those of the best thermoelectric polymers and an order of magnitude smaller than that for Bi_2Te_3. To understand the factors that dominate this low thermal conductivity, we used molecular dynamics simulations to calculate κ_l of crystalline $Cu_3(BTC)_2$ and $TCNQ@Cu_3(BTC)_2$, obtaining a κ_l of 0.58 $Wm^{-1}K^{-1}$ for the uninfiltrated crystalline MOF and 3.84 ± 0.27 $Wm^{-1}K^{-1}$ for the infiltrated crystalline MOF. The addition of TCNQ significantly increases κ_l, which is, at least in part, due to the

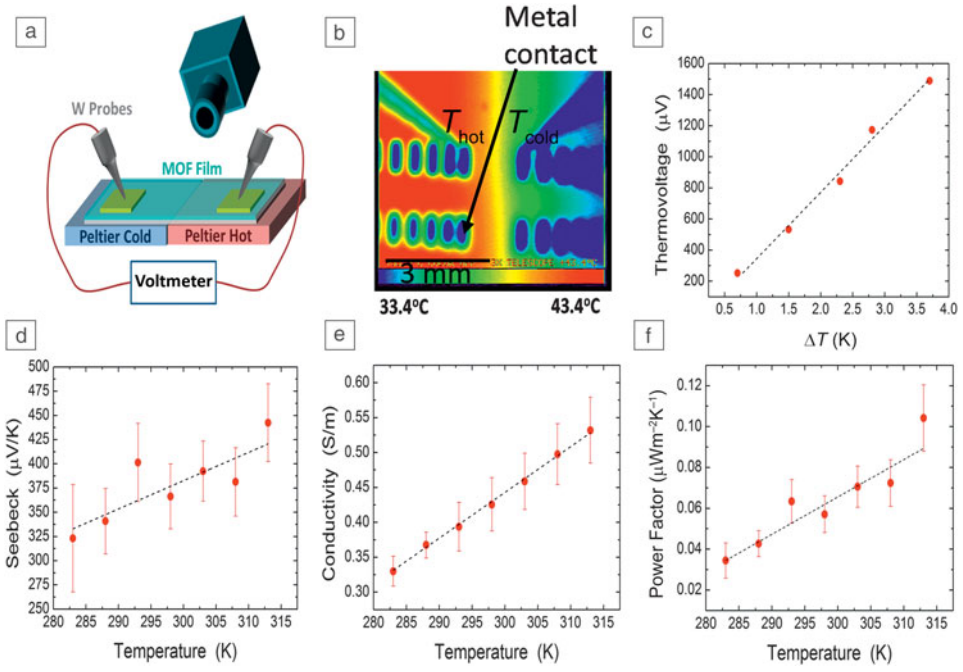

Figure 2. Thermoelectric characterization of metal–organic framework (MOF) thin-film devices. (a) Two Peltier coolers are used to heat and cool the two sides of the substrate, and an infrared (IR) camera is used to measure the temperature *T* profile. (b) IR image taken during one of the measurements. The electrical contacts appear cold in the image because of their different emissivity compared with the MOF. (c) Measured voltage as a function of ΔT (where $\Delta T = T_{hot} - T_{cold}$). The Seebeck coefficient *S* is extracted from the linear fit. (d) *S* as a function of *T*. The dashed line is a linear fit. (e) Electrical conductivity σ as a function of *T*. The dashed line is a linear fit that could represent a thermally activated process with activation energy of 50 meV. (f) Power factor as a function of *T*. The dashed line is a linear fit. The low value of the power factor is largely due to low electrical conductivity. Reprinted with permission from Reference 24. © 1999 Taylor & Francis.

increased density of phonons in the low-frequency/high-group-velocity range. The fact that the calculated values are for a single crystal rather than a polycrystalline material accounts for some of the differences with the experimental values.

Inserting the experimental values we measured for *S*, σ (=0.45 S/m), and κ in Equation 1, we obtain $ZT \approx 7\times10^{-5}$ at 298 K, a value well below those of the best inorganic thermoelectric materials (see Table I). While *S* for the MOF is more than five times larger than that for PEDOT:PSS and κ_l is comparable, it is clear that σ for TCNQ@Cu_3(BTC)$_2$ is the main reason for the reduced performance. Improving crystallinity will likely increase σ, but may also increase κ.

Thermal transport in MOFs

A maximum ratio of σ/κ, which appears in Equation 1, is a goal in designing an ideal TE material, giving rise to the well-known quest for a phonon-glass/electron crystal. (In other words, a material that maximizes phonon scattering, leading to the phonon-mediated thermal conductivity, κ_l, while minimizing electron or hole scattering, leading to both the electrical conductivity, σ, and the electronically mediated thermal conductivity, κ_e.)[23] The quest to synthesize solids with ultralow κ_l has focused on disordered or amorphous phases where structural periodicity and thus phonons (in the strict definition of this quasiparticle) are absent.[24] In this case, the length scales of vibrational energy exchange that contribute to the thermal conductivity can be on the order of the atomic spacing,[25–27] akin to Einstein's original theory of how energy moves through solids.[28,29] However, introducing disorder in the atomic structure may also have detrimental effects on σ. Therefore, maintaining crystallinity while reducing κ_l via limiting the length scales of vibrational energy transfer and other means is a more viable path to achieving maximal material *ZT*.

In the context of the widely adopted kinetic theory, we know that low $\kappa_l = 1/3\ \Sigma_m\ (cv\ell)_m$ results from weak bonding, high atomic mass, complex atomic structures, and high anharmonicity, each of which systematically decreases *c*, the heat carried per mode *m*; *v*, the speed of propagation; and ℓ, the mean free path of the carrier, via different nanoscale mechanisms. MOFs are composed of a variety of atomic species with different masses and heterogeneous bonds. This heterogeneity in masses and bond stiffness directly affects ℓ for any given phonon mode leading to low κ_l. Huang et al.[30] calculated that the intrinsic κ_l of MOF-5 is 0.3 $Wm^{-1}K^{-1}$, resulting from a characteristic ℓ = 0.83 nm, which is considerably smaller than the lattice constant of 2.6 nm and relatively independent of temperature. Wang et al.[31] also used first-principles calculations to determine that, due to its large and complex unit cell, MOF-74 has a large population of optical phonons, which result in more than 50% of the energy being carried by phonons with ℓ < 2 nm.

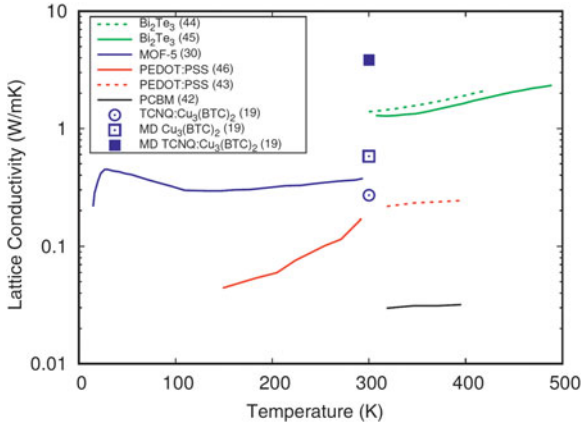

Figure 3. Lattice thermal conductivity κ_l as a function of temperature *T* for several materials. All of these materials display little temperature dependence because of their atomic structure. Note: MOF, metal–organic framework; PEDOT, poly(3,4-ethylenedioxythiophene); PSS, polystyrene sulfonate; PCBM, [6,6]-phenyl-C_{61}-butyric acid methyl ester; TCNQ, tetracyanoquinodimethane; BTC, benzene 1,3,5-tricarboxylate; MD, molecular dynamics.

The open, mechanically soft structure of MOFs leads to relatively low-energy propagation velocities. Huang et al.[30] calculated an atomic density of 24.6 atoms/nm^3 and a sound speed of 1184 m/s for MOF-5. The open structure and large-porosity ratios in MOFs can lead to strong scattering of all phonons at near room temperature, resembling the phonon-glass concept, and a heat capacity that is below the upper, classical limit given by Dulong-Petit.[32] However, it is important to note that increasing the porosity of a MOF will likely have detrimental effects on electrical conductivity and hence *ZT*.

The introduction of guest molecules into MOFs can have a variety of effects on κ_l. Weakly interacting, light molecules such as infiltrated water will likely have no significant effect unless they are in abundance; however, heavier, loosely bound rattling atoms in the MOF pores can significantly reduce κ_l, as has been previously observed for zeolites, skutterudites, and clathrates.[33–38] In particular, "rattlers" reduce κ_l due to the creation of localized modes, enhancement of anharmonicity, and reduction of group velocities.[38] Indeed, acoustic phonons in MOFs have been described to exhibit "rattling-like behavior," which results in exceptionally high anharmonicity of these modes.[38] This implies that the acoustic modes in MOFs could be close to the situation where phonons are "equally strongly damped," as in amorphous and disordered materials.[32,38]

Furthermore, while the use of infiltration to achieve the Guest@MOF can lead to bond stiffening, the resulting variable and complex bonding environments could, in principle, be tuned to enhance vibrational scattering and reduce ℓ. An increase in bond heterogeneity could increase the "rattling-like" behavior of the acoustic modes, increasing anharmonicity and decreasing thermal transport of the affected modes.[39] The infiltration approach could potentially be engineered to create further reductions in the heat-carrying phonons, while providing significant improvement to σ, as discussed.

The temperature dependence of κ_l is also of interest for TE applications given that the temperature difference (ΔT) between the hot and cold sides may be >100 K. Ordinarily in defect-free, crystalline materials above their Debye temperature, κ_l is dominated by anharmonic phonon scattering (such as Umklapp scattering[40]), which leads to a T^{-1} scaling. However, experimentally measured κ values of typical semiconducting organic materials Bi_2Te_3 and MOF-5 exhibit only slightly increasing trends, similar to glassy/amorphous materials as shown in **Figure 3**.[4,19,41–46]

Summary

The need for low-cost, mechanically flexible, and environmentally friendly TE energy-conversion devices has led to increased attention to organic and hybrid organic–inorganic TE materials. Despite impressive progress, substantial challenges remain to increase charge mobility due to inherent and dopant-induced structural disorder, as well as the scarcity of *n*-type organic conductors. In this article, we have asserted that electrically conducting MOFs could solve the disorder problem common to polymers, providing within a single material the highly ordered structure of inorganic conductors with the tunable properties and low cost of organics. Furthermore, we have used the example of TCNQ@$Cu_3(BTC)_2$ framework to illustrate how structure-inherent nanoscale porosity of MOFs provides a route to tuning the electronic properties of these materials with guest molecules without increasing structural disorder. Although σ of TCNQ@$Cu_3(BTC)_2$ is still too low to make it an attractive TE, the recent emergence of several inherently conducting, porous frameworks whose electronic and thermal transport properties could be further tuned using guest molecule infiltration, makes MOFs and Guest@MOFs promising for further exploration for TE energy-conversion applications.

Acknowledgments

The authors thank A. Cruz for assistance with inkjet printing. This work was supported by the Sandia Laboratory Directed Research and Development Program. Sandia National Laboratories is a multiprogram laboratory managed and operated by Sandia Corporation, a wholly owned subsidiary of Lockheed Martin Corporation, for the US Department of Energy's National Nuclear Security Administration under Contract DE-AC04–94AL85000. P.E.H. is grateful for support from the Army Research Office Grant #W911NF-16–1-0320.

References

1. D.M. Rowe, *Thermoelectrics Handbook: Macro to Nano* (CRC Press, Boca Raton, FL, 2005).
2. J.P. Heremans, V. Jovovic, E.S. Toberer, A. Saramat, K. Kurosaki, A. Charoenphakdee, S. Yamanaka, G.J. Snyder, *Science* **321**, 554 (2008).
3. A. Weathers, Z.U. Khan, R. Brooke, D. Evans, M.T. Pettes, J.W. Andreasen, X. Crispin, L. Shi, *Adv. Mater.* **27**, 2101 (2015).
4. J. Liu, X. Wang, D. Li, N.E. Coates, R.A. Segalman, D.G. Cahill, *Macromolecules* **48**, 585 (2015).
5. P. Sheng, Y. Sun, F. Jiao, C. Di, W. Xu, D. Zhu, *Synth. Met.* **193**, 1 (2014).
6. Y. Sun, P. Sheng, C. Di, F. Jiao, W. Xu, D. Qiu, D. Zhu, *Adv. Mater.* **24**, 932 (2012).
7. B. Poudel, Q. Hao, Y. Ma, Y. Lan, A. Minnich, *Science* **320**, 634 (2008).

8. X.A. Yan, B. Poudel, Y. Ma, W.S. Liu, G. Joshi, H. Wang, Y.C. Lan, D.Z. Wang, G. Chen, Z.F. Ren, *Nano Lett.* **10**, 3373 (2010).
9. M.G. Kanatzidis, *MRS Bull.* **40**, 687 (2015).
10. J.-H. Bahk, H. Fang, K. Yazawa, A. Shakouri, *J. Mater. Chem. C* **3**, 10362 (2015).
11. Q. Zhang, Y. Sun, W. Xu, D. Zhu, *Adv. Mater.* **26**, 6829 (2014).
12. Y. Chen, Y. Zhao, Z. Liang, *Energy Environ. Sci.* **8**, 401 (2015).
13. A.J. Heeger, *Chem. Soc. Rev.* **39**, 2354 (2010).
14. O. Bubnova, Z.U. Khan, H. Wang, S. Braun, D.R. Evans, M. Fabretto, P. Hojati-Talemi, D. Dagnelund, J.B. Arlin, Y.H. Geerts, S. Desbief, D.W. Breiby, J.W. Andreasen, R. Lazzaroni, W.M.M. Chen, I. Zozoulenko, M. Fahlman, P.J. Murphy, M. Berggren, X. Crispin, *Nat. Mater.* **13**, 662 (2014).
15. G.H. Kim, L. Shao, K. Zhang, K.P. Pipe, *Nat. Mater.* **12**, 719 (2013).
16. B. Russ, M.J. Robb, F.G. Brunetti, P.L. Miller, E.E. Perry, *Adv. Mater.* **26**, 3473 (2014).
17. D.M. Pajerowski, T. Watanabe, T. Yamamoto, Y. Einaga, *Phys. Rev. B Condens. Matter* **83**, 153202 (2011).
18. G. Gliemann, H. Yersin, *Struct. Bond.* **62**, 87 (1985).
19. K.J. Erickson, F. Leonard, V. Stavila, M.E. Foster, C.D. Spataru, R.E. Jones, B.M. Foley, P.E. Hopkins, M.D. Allendorf, A.A. Talin, *Adv. Mater.* **27**, 3453 (2015).
20. A.A. Talin, A. Centrone, A.C. Ford, M.E. Foster, V. Stavila, P. Haney, R.A. Kinney, V. Szalai, F. El Gabaly, H.P. Yoon, F. Leonard, M.D. Allendorf, *Science* **343**, 66 (2014).
21. J.-L. Zhuang, D. Ar, X.-J. Yu, J.-X. Liu, A. Terfort, *Adv. Mater.* **25**, 4631 (2013).
22. D.G. Cahill, *Rev. Sci. Instrum.* **75**, 5119 (2004).
23. G.A. Slack, D. Rowe, *CRC Thermoelectrics Handbook* (CRC Press, Boca Raton, FL, 1995).
24. P.B. Allen, J.L. Feldman, J. Fabian, F. Wooten, *Philos. Mag. B* **79**, 1715 (1999).
25. S. Shenogin, A. Bodapati, P. Keblinski, A.J.H. McGaughey, *J. Appl. Phys.* **105**, 034906 (2009).
26. J.M. Larkin, A.J.H. McGaughey, *Phys. Rev. B* **89**, 144303 (2014).
27. J.L. Braun, C.H. Baker, A. Giri, M. Elahi, K. Artyushkova, T.E. Beechem, P.M. Norris, Z.C. Leseman, J.T. Gaskins, P.E. Hopkins, *Phys. Rev. B* **93**, 140201 (2016).
28. A. Einstein, *Ann. Phys.* **35**, 679 (1911).
29. D.G. Cahill, S.K. Watson, R.O. Pohl, *Phys. Rev. B* **46**, 6131 (1992).
30. B. Huang, A. McGaughey, M. Kaviany, *Int. J. Heat Mass Transf.* **50**, 393 (2007).
31. X. Wang, R. Guo, D. Xu, J. Chung, M. Kaviany, B. Huang, *J. Phys. Chem. C*, **119**, 26000 (2015).
32. D.G. Cahill, R.O. Pohl, *Annu. Rev. Phys. Chem.* **39**, 93 (1988).
33. G.S. Nolas, J. Cohn, G. Slack, *Phys. Rev. B* **58**, 164 (1998).
34. G.S. Nolas, J. Poon, M. Kanatzidis, *MRS Bull.* **31**, 199 (2006).
35. A. Bentien, M. Christensen, J. Bryan, A. Sanchez, S. Paschen, F. Steglich, G. Stucky, B. Iversen, *Phys. Rev. B Condens. Matter* **69**, 045107 (2004).
36. A. McGaughey, M. Kaviany, *Int. J. Heat Mass Transf.* **47**, 1799 (2004).
37. X. Shi, H. Kong, C.-P. Li, C. Uher, J. Yang, J. Salvador, H. Wang, L. Chen, W. Zhang, *Appl. Phys. Lett.* **92**, 182101 (2008).
38. T. Tadano, Y. Gohda, S. Tsuneyuki, *Phys. Rev. Lett.* **114**, 095501 (2015).
39. W. Qiu, L. Xi, P. Wei, X. Ke, J. Yang, W. Zhang, *Proc. Natl. Acad. Sci. U.S.A.* **111**, 15031 (2014).
40. C. Kittel, *Introduction to Solid State Physics*, 8th ed. (Wiley Hoboken, NJ, 2015), chap. 4.
41. B.L. Huang, Z. Ni, A. Millward, A.J.H. McGaughey, C. Uher, M. Kaviany, O. Yaghi, *Int. J. Heat Mass Transf.* **50**, 405 (2007).
42. J.C. Duda, P.E. Hopkins, Y. Shen, M.C. Gupta, *Phys. Rev. Lett.* **110**, 015902 (2013).
43. J.C. Duda, P.E. Hopkins, Y. Shen, M.C. Gupta, *Appl. Phys. Lett.* **102**, 251912 (2013).
44. X. Tang, W. Xie, H. Li, W. Zhao, Q. Zhang, M. Niino, *Appl. Phys. Lett.* **90**, 12102 (2007).
45. X.B. Zhao, X.H. Ji, Y.H. Zhang, T.J. Zhu, J.P. Tu, X.B. Zhang, *Appl. Phys. Lett.* **86**, 062111 (2005).
46. X.-F. Jiang, J.-K. Xu, B.-Y. Lu, Y. Xie, R.-J. Huang, L.-F. Li, *Chin. Phys. Lett.* **25**, 6 (2008). □

A. Alec Talin has been a member of the technical staff at Sandia National Laboratories since 2002. He is also an adjunct associate professor of materials science and engineering at the University of Maryland. He received a BA degree in chemistry from the University of California, San Diego in 1989, and a PhD degree in materials science and engineering from the University of California, Los Angeles, in 1995. Prior to joining Sandia, he spent six years at Motorola Labs, and was a project leader at the Center for Nanoscale Science and Technology at the National Institute of Standards and Technology. His research focuses on areas of novel electronic materials, energy storage and conversion, and national security. He is a principal editor of the journal *MRS Communications*. Talin can be reached by phone at 925-294-2495 or by email at aatalin@sandia.gov.

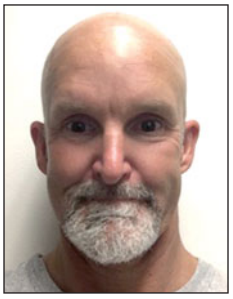

Reese E. Jones is a staff scientist at Sandia National Laboratories. His research ranges from the atomic and molecular scales to the scales at which continuum models become appropriate. Recently, he has been developing and applying methods to interpret and use molecular information in continuum contexts. He has concentrated on extracting transport properties at the nanoscale and devising methods of simulating long-range and large-scale effects on molecular systems. Jones can be reached by email at rjones@sandia.gov.

Patrick E. Hopkins is an associate professor of mechanical and aerospace engineering at the University of Virginia. He was a Harry S. Truman Fellow at Sandia National Laboratories (2008–2011). He received his PhD degree in mechanical and aerospace engineering in 2008, and a BS degree in mechanical engineering and a BA degree in physics in 2004, all from the University of Virginia. He is a recipient of Young Investigator Awards from the Air Force Office of Scientific Research and the Office of Naval Research, The American Society of Mechanical Engineers Bergles-Rohsenow Young Investigator Award in Heat Transfer, and the Presidential Early Career Award for Scientists and Engineers. His interests include thermal-energy transport and photonic interactions in condensed matter, soft materials, liquids, vapors, and their interfaces. Hopkins can be reached by phone at 434-982-6005 or by email at phopkins@virginia.edu.